Pre-Print Manuscript of Article:
Bridgelall, R., "Precision bounds of pavement deterioration forecasts from connected vehicles," *Journal of Infrastructure Systems*, American Society of Civil Engineering, 21(3), pp. 1-7, 2014.

Precision bounds of pavement deterioration forecasts from connected vehicles

Raj Bridgelall, Ph.D.[1]

Abstract

Transportation agencies rely on models to predict when pavements will deteriorate to a condition or ride-index threshold that triggers maintenance actions. The accuracy and precision of such forecasts are directly proportional to the frequency of monitoring. Ride indices derived from connected vehicle sensor data will enable transformational gains in both the accuracy and precision of deterioration forecasts because of very high data volume and update rates. This analysis develops theoretical precision bounds for a ride index called the road impact factor and demonstrates, via a case study, its relationship with vehicle suspension parameter variances.

CE Database subject headings: Deterioration; Forecasting; Intelligent transportation systems; Pavement management; Preservation; Probe instruments; Surface roughness; Vibration

Author Keywords: Connected vehicles; International Roughness Index; Ride quality; Road Impact Factor

1 Introduction

Practitioners have long recognized that rough roads increase vehicle operating costs (Zaniewski and Butler 1985) and lead to more expensive road repairs (AASHTO 2009). Studies have also linked rough roads to motion sickness (Griffin 1990) and higher crash rates (Swedish

[1]Assistant Professor of Transportation and Program Director, Center for Surface Mobility Applications & Real-Time Simulation environments (SMARTSe[SM]), Upper Great Plains Transportation Institute, North Dakota State University, P.O. Box 863676, Plano, TX 75086. Phone: 408-607-3214, E-mail: raj@bridgelall.com

National Road and Transport Research Institute 2004). The ability to accurately predict optimum maintenance cycles has the greatest potential impact on reducing annual maintenance and rehabilitation costs (Madanat, Prozzi and Han 2002). More frequent condition assessments increase the accuracy and precision of predicting when ride-quality indices will reach maintenance thresholds (Haider, Baladi and Chatti 2011). Rural regions that maintain roads suffering rapid deterioration caused by high levels of industrial and agricultural activities will yield the greatest potential benefits from frequent condition assessments (Tolliver and Dybing 2012). Unfortunately, transportation agencies can seldom afford to assess ride-quality more often than once a year. Even so, those assessments are limited to portions of the National Highway System for which the Federal Highway Administration (FHWA) requires annual reporting of the International Roughness Index (IRI) (HPMS 2012). Consequently, agencies miss important vulnerabilities such as frost-heaves that appear and disappear between monitoring cycles.

To provide continuous, network-wide, lower-cost ride-quality measures, the author developed and validated a new approach called the Road Impact Factor (RIF). The average RIF collected from inertial sensors onboard vehicles is directly proportional to the IRI (Bridgelall 2014). Statistically, the RIF variance diminishes exponentially as the volume of sensor readings increase. Using data from inertial sensors in smartphones and connected vehicles to produce the RIF will provide highly precise and continuous ride-quality assessments.

This study characterizes the bounds in forecast precision for common regression models in terms of RIF variability. The latter is a function of motion parameter distributions such as vehicle suspension rates, ground speed, and traversal volume. This is the first study to relate statistics of the RIF to the precision of deterioration forecasts. Related studies use the output of inertial sensors to estimate the IRI by calibrating the acceleration responses of individual vehicles to known values (Nagayama, et al. 2013), or by estimating parameters of an IRI model using neural networks and other methods (Dawkins, et al. 2011).

This paper is organized as follows: Section 2 briefly reviews the RIF model defined in previous research. Section 3 relates the RIF to normalized vertical acceleration energy. Section 4 links statistics of vehicle suspension parameters to the normalized vertical acceleration energy and the RIF. Section 5 derives a model that relates the minimum traversal volume to a level of forecast precision using a common regression model of pavement deterioration. Section 6 presents a case study of the forecast precision bound for a typical distribution of vehicle suspension parameters. Section 7 summarizes and concludes the study.

2 Ride-Index Model

As derived in previous work by the author, the RIF, denoted $R^L[p]$, is the g-force per meter (g/m) experienced when traveling a road segment of length L, during time-period p where:

$$R^L[p] = \sqrt{\frac{1}{L}\int_0^{L/\bar{\sigma}} \left| g_z(t)\sigma(t) \right|^2 dt} \tag{1}$$

The instantaneous traversal speed is $\sigma(t)$ and the on-board sensor output for vertical acceleration is $g_z(t)$.

3 Statistics of Vehicle Response Energy

Road roughness excites the vibration modes of a moving vehicle. The damped mass-spring model for each wheel-suspension assembly or "quarter-car" includes a series combination of sprung and unsprung masses that represent a portion of the body and wheel components respectively. A pair of second-order differential equations characterizes each model. Their solution identifies the dominant resonant frequencies and damping ratios of each mode as functions of the vehicle body mass, wheel mass, spring stiffness, and damping coefficients. These physical parameters must be known to determine the characteristics of each quarter-car mode (Angeles 2011).

The vertical response $z(t)$ to a common broad-band input, namely an impulse, excites all modes equally. The impulse responses of the n under-damped mass-spring systems are:

$$z_{[m,n]}(t) = \frac{U(t)}{\omega_{[m,n]}\sqrt{1-\zeta_{[m,n]}^2}} \exp\left(-\zeta_{[m,n]}\omega_{[m,n]}t\right)\sin\left(\omega_{[m,n]}\sqrt{1-\zeta_{[m,n]}^2}\,t\right) \tag{2}$$

The subscripts $m = 1$ and $m = 2$ enumerate the sprung (s) and unsprung (u) mass-spring subsystem parameters respectively. $U(t)$ is the Heaviside step function. The sprung and unsprung mass resonance frequencies are $\omega_{[s,n]}$ and $\omega_{[u,n]}$ respectively, and their corresponding damping ratios are $\zeta_{[s,n]}$ and $\zeta_{[u,n]}$. The Fourier Transform of the impulse response is a second-order low-pass filter (LPF), $Z(\omega)$, of the form:

$$Z_{[m,n]}(\omega) = \frac{1}{\sqrt{1-\zeta_{[m,n]}^2}} \frac{1}{\left(\omega_{[m,n]}\right)^2 + \left(\zeta\omega_{[m,n]} + j\omega\right)^2} \tag{3}$$

At the sensor's location, the vertical acceleration G_α is a product of the sensor frequency response $S(f)$ and the vector sum of responses from each quarter-car. A linear combination of the mass-spring models for each wheel-assembly produces an equivalent but more analytically convenient model of the acceleration vector, G_β as illustrated in Figure 1. Hence, the magnitude spectrum of the composite vertical acceleration response is:

$$\left|G_\beta(f)\right| = \left|S(f)\right| \sum_{n=1}^{W}\sum_{m=1}^{2} \beta_{[m,n]} \frac{1}{4\pi^2} \frac{1}{\sqrt{1-\zeta_{[m,n]}^2}} \frac{1}{\sqrt{\left(\left[f_{[m,n]}^2 - f^2\right]^2 + \left[2\zeta_{[m,n]}f_{[m,n]}f\right]^2\right)}} \tag{4}$$

The frequencies in hertz are $f_{[m,n]} = \omega_{[m,n]}/2\pi$. W is the number of wheel-spring assemblies and $\beta_{[m,n]}$ are the coefficients of the linear combination. The LPF filter gains are:

$$A_{[m,n]} = \frac{1}{4\pi^2\sqrt{\left(1-\zeta_{[m,n]}^2\right)}} \tag{5}$$

Solving for the sprung and unsprung mass filter coefficients $\beta_{[s,n]}$ and $\beta_{[u,n]}$ respectively such that the energy of G_β equals the energy of G_α yields:

$$\beta_{[s,n]} = \frac{A_{[s,n]}A_{[u,n]}}{A_{[s,n]} + \rho_{[n]}A_{[u,n]}} = \frac{1}{4\pi^2\left[\rho_{[n]}\sqrt{\left(1-\zeta_{[s,n]}^2\right)} + \sqrt{\left(1-\zeta_{[u,n]}^2\right)}\right]} \tag{6}$$

and

$$\beta_{[u,n]} = \frac{A_{[s,n]}A_{[u,n]}}{A_{[s,n]}\,{}^{1}\!/_{\rho_{[n]}} + A_{[u,n]}} = \frac{1}{4\pi^2\left[\sqrt{\left(1-\zeta_{[s,n]}^2\right)} + {}^{1}\!/_{\rho_{[n]}}\sqrt{\left(1-\zeta_{[u,n]}^2\right)}\right]} \tag{7}$$

where the ratios:

$$\rho_{[n]} = \frac{\beta_{[u,n]}}{\beta_{[s,n]}} \tag{8}$$

depends on the vehicle design and sensor installation. Figure 2 plots the Discrete Fourier Transform (DFT) of the vertical acceleration signal samples $\{g_z\}$ obtained from a passenger car used in related studies. A least squares fit of the quarter-car model in Equation (4) with W = 1 provided a ratio of $\rho = 2.4$. The sprung and unsprung mass resonant modes for each quarter-car are observable near 1.5 and 11 hertz respectively. In related work pending publication by the author, a ratio of $\rho = 4.0$ was observable less than 5% of the time from hundreds of traversals of the same road segment, using several types of passenger vehicles.

The suspension parameters from vehicles traversing a road segment will result in a statistical distribution of impulse responses with vertical acceleration energy:

$$E_{[m,n]} = \int_0^\infty \left| g_{[m,n]}(t) \right|^2 dt = \int_0^\infty \left| \frac{d^2}{dt^2} z_{[m,n]}(t) \right|^2 dt = \omega_{[m,n]} \left(\zeta_{[m,n]} + \frac{1}{4\zeta_{[m,n]}} \right) \tag{9}$$

where $g_{[m,n]}$ are the vertical accelerations from the individual mass-spring impulse responses. The vertical acceleration vector at the sensor's position is:

$$g_z(t) = \sum_{n=1}^{W} \sum_{m=1}^{2} \beta_{[m,n]} g_{[m,n]}(t) \tag{10}$$

Therefore, the corresponding acceleration energy E_{gz} is:

$$E_{gz} = \sum_{n=1}^{W} \sum_{m=1}^{2} \int_0^\infty \left| \beta_{[m,n]} g_{[m,n]}(t) \right|^2 dt = \sum_{n=1}^{W} \sum_{m=1}^{2} \beta_{[m,n]}^2 \omega_{[m,n]} \left(\zeta_{[m,n]} + \frac{1}{4\zeta_{[m,n]}} \right) \tag{11}$$

From the theory of error propagation (Ku 1966), the acceleration energy variance is:

$$vE_{gz} = \sum_{n=1}^{W} \sum_{m=1}^{2} \left[\left(\frac{\partial E_{gz}}{\partial \omega_{[m,n]}} \right)^2 s_{\omega[m,n]}^2 + \left(\frac{\partial E_{gz}}{\partial \zeta_{[m,n]}} \right)^2 s_{\zeta[m,n]}^2 + \left(\frac{\partial E_{gz}}{\partial \omega_{[m,n]}} \right) \left(\frac{\partial E_{gz}}{\partial \zeta_{[m,n]}} \right) s_{\omega\zeta[m,n]}^2 \right] \tag{12}$$

where $s_{\omega[m,n]}^2$, $s_{\zeta[m,n]}^2$ and $s_{\omega\zeta[m,n]}^2$ are the variances of the mode resonant frequencies, damping ratios, and their covariance factors respectively. The latter is zero because the resonant frequencies and damping ratios are statistically independent. Substituting the partial derivatives indicated yield:

$$vE_{gz} = \sum_{n=1}^{W} \sum_{m=1}^{2} \left[\beta_{[m,n]}^4 \left(\zeta_{\mu[m,n]} + \frac{1}{4\zeta_{\mu[m,n]}} \right)^2 s_{\omega[m,n]}^2 + \left(\nabla E_{\zeta[m,n]} \right)^2 s_{\zeta[m,n]}^2 \right] \tag{13}$$

where

$$\nabla E_{\zeta[s,n]} = \frac{2\rho_{[n]}^{3}\omega_{[u,n]}\zeta_{[s,n]}^{3}\left(4\zeta_{[u,n]}^{2}+1\right)+\omega_{[s,n]}\zeta_{[u,n]}\left\{\rho_{[n]}\left[\zeta_{[s,n]}^{2}\left(4\zeta_{[s,n]}^{2}+7\right)-1\right]+\sqrt{\left(1-\zeta_{[s,n]}^{2}\right)\left(1-\zeta_{[u,n]}^{2}\right)}\left(4\zeta_{[s,n]}^{2}+1\right)\right\}}{64\pi^{2}\zeta_{[s,n]}^{2}\zeta_{[u,n]}\left\{\rho_{[n]}\sqrt{1-\zeta_{[s,n]}^{2}}+\sqrt{1-\zeta_{[u,n]}^{2}}\right\}^{3}\sqrt{1-\zeta_{[s,n]}^{2}}} \tag{14}$$

and

$$\nabla E_{\zeta[u,n]} = \frac{2\omega_{[s,n]}\zeta_{[u,n]}^{3}\left(4\zeta_{[s,n]}^{2}+1\right)+\rho_{[n]}^{2}\omega_{[u,n]}\zeta_{[s,n]}\left\{\zeta_{[u,n]}^{2}\left(4\zeta_{[u,n]}^{2}+7\right)+\rho_{[n]}\left(4\zeta_{[u,n]}^{2}-1\right)\sqrt{\left(1-\zeta_{[s,n]}^{2}\right)\left(1-\zeta_{[u,n]}^{2}\right)}-1\right\}}{64\pi^{2}\zeta_{[s,n]}\zeta_{[u,n]}^{2}\left\{\rho_{[n]}\sqrt{1-\zeta_{[s,n]}^{2}}+\sqrt{1-\zeta_{[u,n]}^{2}}\right\}^{3}\sqrt{1-\zeta_{[u,n]}^{2}}} \tag{15}$$

This energy variance is an important factor of the RIF variance derived in the next section.

4 RIF Variance

From Equation (1), the κth traversal of a road segment traveled at an average speed $\overline{\sigma}_{\kappa}$ produces a RIF of:

$$R_{\overline{\sigma}}^{L} = \overline{\sigma}_{\kappa}\sqrt{\frac{1}{L}\int_{0}^{L/\overline{\sigma}}\left|g_{z}(t)\right|^{2}dt} = \overline{\sigma}_{\kappa}\sqrt{\frac{1}{L}}\sqrt{\lim_{\varepsilon\to 0}\int_{0}^{T_{\varepsilon}}\left|g_{z}(t)\right|^{2}dt} = \overline{\sigma}_{\kappa}\sqrt{\frac{1}{L}}\sqrt{E_{gz}} \tag{16}$$

where $T_{\varepsilon} = |g_{z}^{-1}(\varepsilon)|$. That is, the limit of integration is when the vertical acceleration of the impulse response vector becomes negligibly small. The standard deviation of the RIF, s_{RIF}^{L} is, therefore:

$$s_{RIF}^{L} = \sqrt{\left(\frac{\partial R_{\overline{\sigma}}^{L}}{\partial \overline{\sigma}_{\kappa}}\right)^{2} v\left[\overline{\sigma}_{\kappa}\right] + \left(\frac{\partial R_{\overline{\sigma}}^{L}}{\partial E_{gz}}\right)^{2} vE_{gz} + \left(\frac{\partial R_{\overline{\sigma}}^{L}}{\partial \overline{\sigma}_{\kappa}}\right)\left(\frac{\partial R_{\overline{\sigma}}^{L}}{\partial E_{gz}}\right)s_{\overline{\sigma}E}^{2}} \tag{17}$$

where $v\left[\overline{\sigma}_{\kappa}\right]$ is the variance of the mean speed among traversals. The covariance of the mean speed and the vertical acceleration signal energy, denoted $s_{\overline{\sigma}E}^{2}$, is zero because of their statistical independence. Evaluating the partial derivates indicated in Equation (17) yields:

$$s_{RIF}^{L} = \sqrt{\frac{1}{L}\left(\overline{E}_{gz} v[\overline{\sigma}_{\kappa}] + \frac{\left(\overline{\overline{\sigma}}_{\kappa}/2\right)^{2}}{\overline{E}_{gz}} vE_{gz}\right)} \tag{18}$$

where $\overline{E}_{gz}$ and $\overline{\overline{\sigma}}_{\kappa}$ are respectively the mean vertical acceleration signal energy and the mean of the average speed among traversals. This expression establishes a variance boundary for the independent parameter of any related regression model used to predict a future deterioration threshold.

5 Deterioration Forecasting Models

The most common models of pavement deterioration are empirical regression of the IRI because they provide the greatest practical value and abstract the complexity of the underlying phenomena (Lu and Tolliver 2012). Research demonstrates that IRI over time follows the exponential form (S. W. Haider, et al. 2010):

$$\psi(t) = \psi_0 \exp(\beta_L t) \tag{19}$$

where ψ_0 and $\psi(t)$ are respectively the initial and expected ride-indices at time t, and β_L is a calibration parameter that best fits the historical ride-index measured for segment L. Therefore, the expected time to reach a given index threshold ψ_α is:

$$\hat{T}(\psi_\alpha) = \frac{1}{\beta_L}\ln\left(\frac{\psi_\alpha}{\psi_0}\right) \tag{20}$$

The estimate uncertainty for a future time, $s_{T\psi}$, to reach the ride-index threshold is:

$$s_{T\psi} = \sqrt{\left[\frac{\partial T(\psi_\alpha)}{\partial \psi_\alpha}\right]^2 s_{\psi\alpha}^2} = \frac{1}{\beta_L}\frac{s_{\psi\alpha}}{\psi_\alpha} \tag{21}$$

where $s_{\psi\alpha}$ is a window of uncertainty about the future ride-index threshold. Using RIF as the ride-index, the ratio $s_{\psi\alpha}/\psi_\alpha$ is bounded by the ratio of the RIF standard deviation to the mean RIF of quarter-car impulse responses where:

$$\frac{s_{\psi\alpha}}{\psi_\alpha} = \frac{s^L_{RIF}}{R^L_{\bar{\sigma}}} = \sqrt{\frac{v[\bar{\sigma}_\kappa]}{\bar{\bar{\sigma}}_k^2} + \frac{1}{4}\frac{vE_{gz}}{\bar{E}_{gz}^2}} \tag{22}$$

The time margin-of-error ΔT_ψ is:

$$\Delta T_\psi = \frac{q_{1-\alpha/2} \times s_{T\psi}}{\sqrt{N_\upsilon}} = \frac{q_{1-\alpha/2}}{\sqrt{N_\upsilon}} \frac{1}{\beta_L} \frac{s^L_{RIF}}{R^L_{\bar{\sigma}}} \tag{23}$$

where N_υ is the traversal volume, and $q_{1-\alpha/2}$ is the standard normal quantile for a (1-α)% confidence interval (Papoulis 1991). Therefore, the minimum traversal volume needed to achieve a minimum desired precision (maximum ΔT_ψ) of the estimated time when the pavement will deteriorate to a future ride-index ψ is:

$$N_\upsilon(\Delta T_\psi) = \left(\frac{1}{\Delta T_\psi}\frac{q_{1-\alpha/2}}{\beta_L}\right)^2 \left(\frac{v[\bar{\sigma}_\kappa]}{\bar{\bar{\sigma}}_k^2} + \frac{1}{4}\frac{vE_{gz}}{\bar{E}_{gz}^2}\right) \tag{24}$$

Given a deterioration rate parameter β_L, the precision ΔT_ψ is bounded by the sum of the standard deviation-to-mean value ratios of the traversal velocity and vertical acceleration signal energy respectively. The latter is bounded by the variance of the impulse response energy relative to the mean response energy for all the vehicles that traverse the monitored road segment.

6 Case Study

6.1 Vehicle Suspension Statistics

It is standard practice for vehicle manufacturers to attenuate the vertical motion between 4 and 8 hertz because vibration levels within that frequency range are the most harmful to humans

(Griffin 1990). To achieve this, manufacturers distribute the sprung and unsprung masses so that they account for 90% and 10% respectively of the gross vehicle weight (Gillespie 2004). The average curb weight of vehicles increased steadily since 1985 and peaked in 2007 (Bastani, Heywood and Hope 2012), but trends indicate that they will return to 1990 levels by 2015. The average gross mass, $m_{\mu G}$, for vehicles manufactured in 2007 was 2226 kilograms and the standard deviation, s_{mG}, was 483.7 kilograms (Woodyard 2007). These yield the mean and standard deviations of the quarter-car sprung and unsprung masses, m_s and m_u respectively.

Suspension system engineers also design the sprung mass resonant frequency between 0.9 and 1.5 hertz for all vehicle types (General Motors 1987). If this is approximately the six-sigma range for normally distributed sprung mass resonant frequencies, ω_s, of vehicles that travel any road segment, then the mean frequency and standard deviation are 1.2 and 0.1 hertz respectively. Similarly, vehicle suspension shock absorbers produce sprung mass damping ratios, ζ_s, in the range of 0.3 to 0.4 (Gillespie 2004). Hence the mean and standard deviation for a normal distribution is 0.35 and 0.017 respectively.

A tire at its rated load will experience a deflection of approximately 25 mm (Gillespie 2004), therefore, for four-wheeled vehicles, an estimate of the average unsprung mass spring stiffness, k_u, in units of N·m^{-1} is:

$$k_u = \frac{(m_{\mu G}/4)g}{0.025} \qquad (25)$$

where g is the g-force constant of 9.8 m·s^{-2}. The mean unsprung mass resonant frequency, ω_u, is therefore:

$$\omega_u = \sqrt{\frac{k_u}{m_u}} \qquad (26)$$

where m_u is the average unsprung mass. From the gross mass statistics above, the associated average resonant frequency is approximately 10 hertz. Its standard deviation is:

$$s_{\omega u} = \sqrt{\left(\frac{\partial \omega_u}{\partial k_u}\right)^2 s_{ku}^2 + \left(\frac{\partial \omega_u}{\partial m_u}\right)^2 s_{mu}^2 + \left(\frac{\partial \omega_u}{\partial k_u}\right)\left(\frac{\partial \omega_u}{\partial m_u}\right) s_{km}^2} \tag{27}$$

For this scenario, both k_u and m_u depend on the gross vehicle mass statistics, therefore, the covariance factor is unity and the expression becomes:

$$s_{\omega u} = \sqrt{\frac{1}{4k_u m_u} s_{ku}^2 + \frac{k_u}{4m_u^3} s_{mu}^2 - \frac{1}{4m_u^2}} \tag{28}$$

The average damping ratio for the unsprung mass is defined as:

$$\zeta_u = \frac{c_u}{2\sqrt{m_u k_u}} = \frac{c_u}{2m_u \omega_u} \tag{29}$$

The unsprung mass damping coefficient c_u is typically $\eta = 15\%$ of the sprung mass damping coefficient c_s (Türkay and Akçay 2008). Therefore,

$$\zeta_u = \frac{\eta c_s}{2m_u \omega_u} = \frac{\eta(2m_s \omega_s \zeta_s)}{2m_u \omega_u} = \eta \zeta_s \frac{m_s}{m_u} \frac{\omega_s}{\omega_u} \tag{30}$$

where m_s, ω_s, and ζ_s are the means of the sprung masses, their resonant frequencies, and their damping ratios respectively. Hence, the standard deviation of the unsprung mass damping ratio is:

$$s_{\zeta u} = \sqrt{\left(\frac{\partial \zeta_u}{\partial \zeta_s}\right)^2 s_{\zeta s}^2 + \left(\frac{\partial \zeta_u}{\partial \omega_s}\right)^2 s_{\omega s}^2 + \left(\frac{\partial \zeta_u}{\partial \omega_u}\right)^2 s_{\omega u}^2 + \left(\frac{\partial \zeta_u}{\partial m_s}\right)^2 s_{ms}^2 + \left(\frac{\partial \zeta_u}{\partial m_u}\right)^2 s_{mu}^2 + \Delta_{cv}} \tag{31}$$

where the covariance term ∇_{cv} is:

$$\Delta_{cv} = \left(\frac{\partial \zeta_u}{\partial m_s}\right)\left(\frac{\partial \zeta_u}{\partial m_u}\right) s_{msmu}^2 + \left(\frac{\partial \zeta_u}{\partial m_s}\right)\left(\frac{\partial \zeta_u}{\partial \omega_u}\right) s_{ms\omega u}^2 + \left(\frac{\partial \zeta_u}{\partial m_u}\right)\left(\frac{\partial \zeta_u}{\partial \omega_u}\right) s_{mu\omega u}^2 \tag{32}$$

For this scenario, the variables m_s, m_u, and ω_u are proportionally linked per the guidelines for typical vehicle suspension designs; therefore, their respective covariance factors s_{msmu}, $s_{ms\omega u}$, and $s_{mu\omega u}$ are unity. Evaluating the partial derivatives indicated, and simplifying yields:

$$\Delta_{cv} = \left(\eta^2 \zeta_s^2 \frac{m_s}{m_u} \frac{\omega_s^2}{\omega_u^2} \right) \left[\frac{m_s - m_u - \omega_u}{m_u^2 \omega_u} \right] \tag{33}$$

With these typical values of vehicle parameters, all of values for the mean and variance of the quarter-car suspension parameters specified in Equations (11) and (13) are now known to compute a value for the energy variance to mean ratio of Equation (18). Table 1 summarizes the ratios of standard deviations to mean values for the sprung and unsprung mass parameters of this case study. With these values, Equation (24) will produce the number of sensor readings needed for a specified level of forecast precision and confidence when given the average traversal speed, its standard deviation, and the historical rate of pavement deterioration. The next section provides an example based on a typical scenario.

6.2 Deterioration Forecasting Example

As shown in Figure 2, estimating a single quarter-car response from the aggregate provides a reasonable simplification to accommodate the quarter-car statistics from the case study. Figure 3 plots Equation (24), normalized to the number of data collection days required for a desired maximum forecast precision within a 95% confidence interval. This result is based on an average travel speed of 24.6 m/s (about 55 mph) within a 5% standard deviation. The number of data collection days depend on the typical Annual Average Daily Traffic (AADT) volume medians of 10,965 and 39,093 passenger cars per lane for rural and urban Interstate functional classifications respectively (Hausman and Clarke 2012), and a scenario where only 20% of the vehicles are equipped with sensors. The result is also based on typical rural and urban interstate highway deterioration rates (Anastasopoulos, Mannering and Haddock 2009), which correspond to β_L values of 0.056 and 0.055 respectively. The plot for this scenario indicates that one week of data collection will forecast RIF thresholds with a worst-case precision of two weeks for the typical urban and rural Interstate. To maintain homoscedasticity, the maximum data collection period selected should be less than the maximum time-period that the deterioration level is relatively unchanged.

7 Summary and Conclusions

The ability to collect and process data from a large number of inertial sensors in a connected vehicle environment will provide transformational gains in the precision and accuracy of forecasting pavement deterioration forecasts. Fundamentally, the accuracy and precision of a regression model's ability to predict pavement deterioration is directly proportional to the rate of its recalibration with new ride-quality data. Statistical properties of the road impact factor (RIF), a new ride-index introduced in previous work, inherently improves its forecast precision as data volume increases, making it an ideal model for a connected vehicle environment. This analysis provides theoretical insights that relate the statistics of vehicle motion parameters to bounds of its forecast precision. The supporting case study used suspension parameter variances published for vehicles manufactured in 2007. A scenario with 20% of the passenger cars traveling a typical U.S. interstate highway at a common speed limit and producing RIF data was analyzed. Results for this scenario indicate that the model will predict a future ride-index within a worst case precision of two weeks from statistics of RIF data collected for about one week.

Future work will characterize pavement distress symptom location accuracy in terms of the variability of vehicle suspension response durations, errors in geospatial position estimates, and asynchronous accelerometer and GPS sample rates.

Acknowledgement

This work is based on research supported by the United Stated Department of Transportation (USDOT), Research and Innovative Technology Administration (RITA) under the Rural Transportation Research Initiative.

Notation

The following symbols are used in this paper:

$A_{[m, n]}$	=	low-pass filter amplitude for mass-spring model n;
c_s	=	average damping coefficient of the sprung mass response motion;
c_u	=	average damping coefficient of the unsprung mass response motion;
f	=	frequency in hertz;
$f_{[s,n]}$	=	sprung mass resonance mode frequency (hertz) of quarter-car n;
$f_{[u,n]}$	=	unsprung mass resonance mode frequency (hertz) of quarter-car n;
$g_z(t)$	=	aggregate g-force output from the inertial sensor as a function of time t;
$g_{[u,n]}(t)$	=	g-force sensed as a function of time t from individual mass-spring models;
k_u	=	unsprung mass spring stiffness;
L	=	length of road segment;
m_s	=	the average sprung mass of vehicles;
m_u	=	the average unsprung mass of vehicles;
$m_{\mu G}$	=	average gross mass for vehicles;
N_v	=	the traversal volume;
$R^L[p]$	=	RIF for segment of length L evaluated in time-period p;
$R^L_{\bar{\sigma}}$	=	RIF for segment of length L when traversed at an average speed $\bar{\sigma}$;
s_{ks}	=	standard deviation of the sprung mass spring stiffness;

s_{ku}	=	standard deviation of the unsprung mass spring stiffness;
s_{km}^2	=	covariance of the unsprung mass and its spring stiffness;
s_{ms}	=	standard deviation of the sprung mass;
s_{mu}	=	standard deviation of the unsprung mass;
s_{msmu}	=	covariance between the sprung mass and the unsprung mass;
$s_{ms\omega u}$	=	covariance between the sprung mass and unsprung mass resonance;
$s_{mu\omega u}$	=	covariance between the unsprung mass and the unsprung mass resonance;
s_{RIF}^L	=	standard deviation of the RIF for segment of length L;
$s_{T\psi}$	=	uncertainty of estimating the future time to reach a ride-index threshold ψ;
$s_{\omega s}$	=	standard deviation of the sprung mass resonant frequency;
$s_{\omega u}$	=	standard deviation of the unsprung mass resonant frequency;
$s_{\psi\alpha}$	=	the uncertainty band about a future ride-index threshold $\psi\alpha$;
$s_{\zeta s}$	=	standard deviation of the sprung mass damping ratio;
$s_{\zeta u}$	=	standard deviation of the unsprung mass damping ratio;
$s_{\bar{\sigma}E}^2$	=	covariance of the average speed and vertical acceleration signal energy;
$s_{\omega[m,n]}^2$	=	variances of the mode resonant frequencies;
$s_{\omega\zeta[m,n]}^2$	=	covariances of the mode resonant frequencies and damping ratios;
$s_{\zeta[m,n]}^2$	=	variances of the mode damping ratios;
$S(f)$	=	inertial sensor frequency response function;
T_ε	=	limit of integration when the vertical acceleration is negligibly small;
$q_{1-\alpha/2}$	=	the standard normal quantile for a (1-α)% confidence interval;

vE_{gz}	=	the variance of acceleration energy;
$v[\bar{\sigma}_\kappa]$	=	the variance of the mean speed among κ traversals;
W	=	the number of vehicle wheel-spring assemblies;
$U(t)$	=	the Heaviside step function;
$z_{[m,n]}(t)$	=	vertical motion of each mass-spring model;
$Z_{[m,n]}(\omega)$	=	Fourier transform of the vertical motion of each mass-spring model;
$\beta_{[u,n]}$	=	proportion of each LPF in the linear combination aggregate model;
β_L	=	a calibration parameter that best fits the segment L ride-index time series;
∇_{cv}	=	expression of the covariance factors among parameters;
$\Delta \mathrm{T}_\psi$	=	the time margin-of-error relative to the ride-index standard deviation;
$\rho_{[u,n]}$	=	ratio of unsprung to sprung mass quarter-car model n coefficient;
$\bar{\sigma}_\kappa$	=	average or constant speed for the κ^{th} traversal;
$\bar{\bar{\sigma}}_\kappa$	=	mean of the average or constant speed among traversals;
$\sigma(t)$	=	instantaneous traversal speed as a function of time;
ω_s	=	average sprung mass angular resonance frequency;
ω_u	=	average unsprung mass angular resonance frequency;
$\omega_{[s,n]}$	=	sprung mass resonance mode angular frequency of quarter-car n;
$\omega_{[u,n]}$	=	unsprung mass resonance mode angular frequency of quarter-car n;
ψ_0	=	the initial ride-index at time $t = 0$;
ψ_α	=	a ride-index threshold that triggers maintenance action;
$\psi(t)$	=	the expected ride-index at time t;
ζ_s	=	average damping ratio of the sprung sprung mass frequency response;

ζ_u	=	average damping ratio of the unsprung sprung mass frequency response;
$\zeta_{[s,n]}$	=	damping ratios of the sprung mass frequency response;
$\zeta_{[u,n]}$	=	damping ratios of the unsprung mass frequency response.

References

AASHTO. *Rough Roads Ahead: Fix Them Now or Pay for It Later.* Washington, DC: American Association of State Highway and Transportation Officials (AASHTO) and The Road Information Program (TRIP), 2009.

Anastasopoulos, Panagiotis Ch., Fred L. Mannering, and John Haddock. *Effectiveness and Service Lives/Survival Curves of Various Pavement Rehabilitation Treatments.* Publication FHWA/IN/JTRP-2008/12. Joint Transportation Research Program, Indiana: Indiana Department of Transportation and Purdue University, 2009.

Angeles, Jorge. *Dynamic Response of Lineaer Mechanical Systems: Modeling, Analysis and Simulation.* New York: Springer, 2011.

Bastani, Parisa, John B. Heywood, and Chris Hope. *U.S. CAFE Standards -- Potential for Meeting Light-duty Vehicle Fuel Economy Targets, 2016-2025.* MIT Energy Initiative, Boston, Massachusetts: Massachusetts Institute of Technology, 2012.

Bridgelall, Raj. "Connected Vehicle Approach for Pavement Roughness Evaluation." *Journal of Infrastructure Systems* (American Society of Civil Engineers) 20, no. 1 (April 2014): 04013001.

Dawkins, Jeremy, David Bevly, Buzz Powell, and Richard Bishop. *Investigation of Pavement Maintenance Applications of Intellidrive.* Pooled Fund Study, Charlottesville, Virginia: University of Virginia, 2011.

General Motors. *Suspension Rates and Frequency.* Suspension Design Guidelines 1070, Detroit, Michigan: General Motors, 1987.

Gillespie, Thomas D. *CarSim Data Manual.* Ann Arbor, Michigan: Mechanical Simulation Corporation, 2004.

Griffin, M. J. *Handbook of Human Vibration.* New York: Elsevier, 1990.

Haider, Sayed Waqar, Gilbert Y. Baladi, Karim Chatti, and Christopher M. Dean. "Effect of Pavement Condition Data Collection Frequency on Performance Prediction." *Transportation Research Record: Journal of the Transportation Research Board* (Transportation Research Board), no. 2153 (2010): 67-80.

Haider, Syed Waqar, Gilbert Y. Baladi, and Karim Chatti. "Impact of Pavement Surface Monitoring Frequency on Pavement Management Decision Making." Edited by Imad Al-Qadi and Scott Murrell. *Transportation and Development Institute Congress 2011.* Chicago, Illinois: American Society of Civil Engineers, 2011. 656-666.

Hausman, Joseph, and Justin Clarke. *FHWA Functional Classification Guidance Update.* Report, Federal Highway Administration, Washington, DC: U.S. Department of Transportation, 2012.

HPMS. Highway Performance Monitoring System Field Manual (HPMS), Office of Highway Policy Information Federal Highway Administration, Washington, DC: Federal Highway Administration, 2012.

Ku, Harry H. "Notes on the Use of Propagation of Error Formulas." *Journal of Research of the National Bureau of Standards, Section C: Engineering and Instrumentation* (National Bureau of Standards) 70C, no. 4 (1966): 263-273.

Lu, Pan, and Denver Tolliver. "Pavement Pre- and Post-Treatment Performance Models Using LTPP Data." *Journal of the Transportation Research Forum* (Transportation Research Forum) 51, no. 3 (2012): 67-81.

Madanat, Samer, Jorge A. Prozzi, and Michael Han. "Effect of Performance Model Accuracy on Optimal Pavement Design." *Computer-Aided Civil and Infrastructure Engineering* 17, no. 1 (January 2002): 22-30.

Nagayama, Tomonori, Akira Miyajima, Shunya Kimura, Yuuki Shimada, and Yozo Fujino. "Road condition evaluation using the vibration response of ordinary vehicles and synchronously recorded movies." *Proceedings of the SPIE 8692, Sensors and Smart Structures Technologies for Civil, Mechanical, and Aerospace Systems 2013.* Bellingham, Washington: International Society for Optics and Photonics (SPIE), 2013.

Papoulis, Athanasios. *Probalility, Random Variables, and Stochastic Processes.* New York: McGraw-Hill, 1991.

Swedish National Road and Transport Research Institute. "The influence of road surface condition on traffic safety and ride comfort." *Sixth International Conference on Managing Pavements: The Lessons, The Challenges, The Way Ahead.* Brisbane, Queensland, Australia: Queensland Department of Main Roads, 2004.

Tolliver, Denver, and Alan Dybing. *An Assessment of County and Local Road Infrastructure Needs in North Dakota.* Research Report, Upper Great Plains Transportation Institute (UGPTI), Fargo: North Dakota State University (NDSU), 2012.

Türkay, Semiha, and Hüseyin Akçay. "Influence of tire damping on the ride performance potential of quarter-car active suspensions." *47th IEEE Conference on Decision and Control.* New York, New York: Institute of Electrical and Electronic Engineers (IEEE), 2008.

Woodyard, Chris. *Vehicles keep inching up and putting on pounds.* July 16, 2007. http://usatoday30.usatoday.com/money/autos/2007-07-15-little-big-cars_N.htm (accessed March 14, 2014).

Zaniewski, John P., and Bert C. Butler. "Vehicle Operating Costs Related to Operating Mode, Road Design, and Pavement Condition." In *Measuring Road Roughness and Its Effects on User Cost and Comfort*, edited by Thomas D. Gillespie and Michael Sayer, 127-142. Philadelphia: American Society for Testing and Materials, 1985.

360 **Figures**

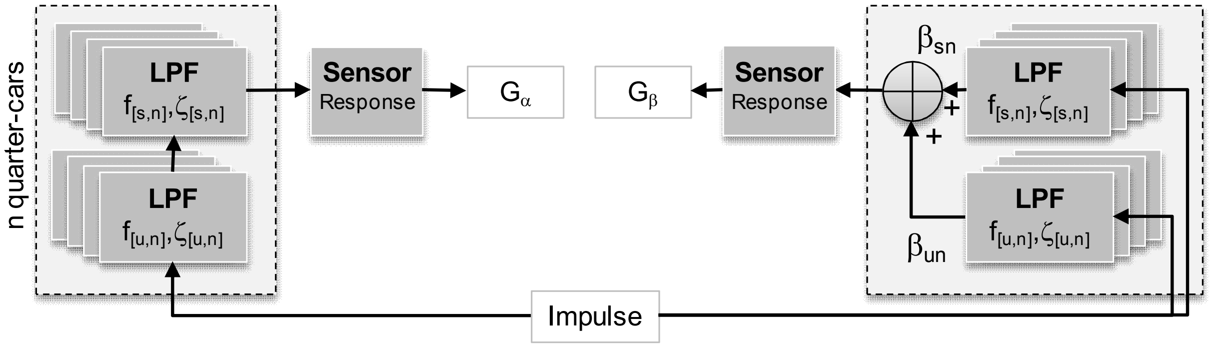

Figure 1. Equivalent response models of vehicle dynamics

361

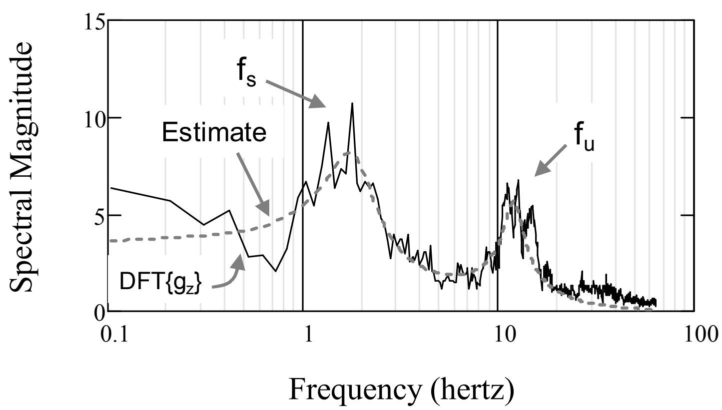

Figure 2. DFT of sensor output versus estimate of the quarter-car response

362

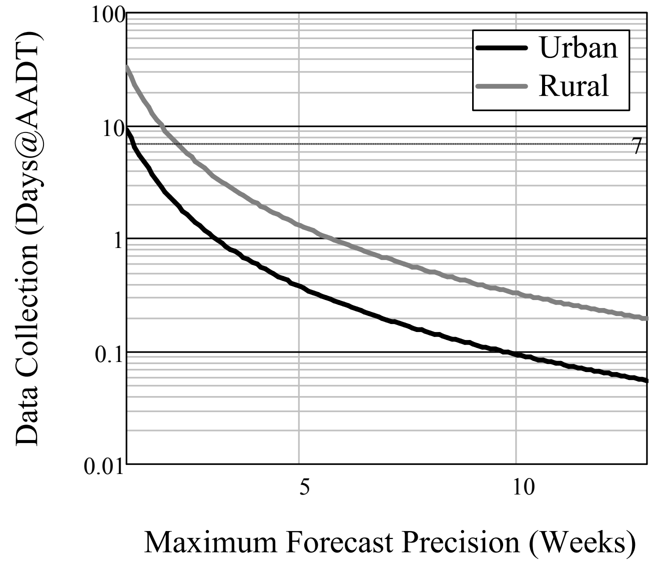

Figure 3. Data collection time needed for a desired maximum forecasting precision

Table 1: Ratio of standard deviation to the mean value for typical vehicles

Parameter	Sprung Mass	Unsprung Mass
Resonant Frequency (ω)	8.3%	15.4%
Damping Ratio (ζ)	4.8%	35.7%
Spring Stiffness (*k*)	27.4%	21.7%
Damping Coefficient (*c*)	18.1%	18.1%